Overall Considerations on the Quenching of PH$_2$(Ã^{2}A$_1$) and New Effects in Collision-Induced V−V Energy Transfer of PH$_2$(X̃^{2}B$_1$; $v_2'' = 1$)

Chieu Nguyen Xuan*

Istituto di Metodologie Inorganiche e dei Plasmi, Consiglio Nazionale delle Ricerche,
Area della Ricerca di Roma 1, Via Salaria Km 29,300, 00016 Monterotondo Scalo (Roma), Italy

The quenching constants of PH$_2$(Ã^{2}A$_1$; $v_2' = 0$ and 1) by H$_2$S, NH$_3$, COS, CHCl$_3$, and CH$_4$ have been measured. Attempts to correlate these data and those published in previous papers due to other quenchers, with the molecular properties through the Parmenter and co-workers' theory, the Thayer and Yardley's model, and the collision complex formation theory have been made. Measurements of collision-induced deactivation constants of PH$_2$(X̃^{2}B$_1$; $v_2'' = 1$) by COS, CHCl$_3$, and CH$_4$ have also been carried out. A reliable linear relationship of the log values of V−V energy exchange probability with the minimum energy mismatch Δv between PH$_2$($v_2'' = 1$) and the quenchers has been shown. Effects on the V−V transfer efficiency by inversion doubling of NH$_3$ and by the degenerate vibrational modes of the quencher, which participate in the process, have been evidenced.

1. Introduction

Collisional deactivation of the excited Ã^{2}A$_1$ electronic state and of the bending $v_2'' = 1$ level of the ground X̃^{2}B$_1$ electronic state of the PH$_2$ radical has been extensively studied in this laboratory, and experimental data obtained for numerous quenchers have been reported in previous publications.[1,2] The quenchers so far dealt with are of progressive molecular complexity going from noble atomic gases to simple polyatomic molecules.

Investigations concerning the $v_2' = 0$ and $v_2' = 1$ vibrational levels of PH$_2$(Ã^{2}A$_1$) have been carried out, and the results have been interpreted with the theories by Parmenter et al.[3] and by Thayer and Yardley[4] and also with the theory of collision complex formation.[5]

Data obtained for the vibrational relaxation of the $v_2'' = 1$ level of PH$_2$(X̃^{2}B$_1$) are of particular interest. The action of the rare gases have been seen to follow as well the Parmenter et al. theory, revealing a long-range interaction between these atomic gases and the vibrationally excited PH$_2$(X̃^{2}B$_1$; $v_2'' = 1$) species.[6] The NO molecule gives rise with PH$_2$(X̃^{2}B$_1$; $v_2'' = 0$) to a chemical reaction, the kinetics of which is enhanced by a factor 122 when the v_2'' vibrational state is excited by one quantum.[7] Polyatomic quenchers interact with (X̃^{2}B$_1$; $v_2'' = 1$) prevalently through a V−V energy exchange process.[2] Recently, we have been able to show for the first time evidence of the influence of the inversion doubling of NH$_3$ on the V−V exchange between this molecule and PH$_2$(X̃^{2}B$_1$; $v_2'' = 1$).[1]

It has been seen that there is a linear relationship between the log values of deactivation probability of (X̃^{2}B$_1$; $v_2'' = 1$) and the difference in energy between ($v_2'' = 1$) and the frequency of the quencher vibrational mode energetically closest to it, i.e., Δv (cm^{-1}), and responsible for the energy transfer.

This paper extends our investigations on other quenchers in order to settle the just-mentioned linear relationship of the $v_2'' = 1$ deactivation efficiency with Δv on a more solid basis. On

the other hand, a richer corpus of data, in particular those of polar molecules, concerning the quenching of PH$_2$(Ã^{2}A$_1$; $v_2' = 0$ and 1), should be helpful in getting a deeper insight into the mechanisms involved and suggested in the previous articles.

In this work, the quenchers employed are H$_2$S, NH$_3$, COS, CHCl$_3$, and CH$_4$.

2. Experimental

The experimental procedure and apparatus have been described in detail in previous papers,[1,2] hence they will be here only briefly presented.

The PH$_2$ radical was generated by photolysis of PH$_3$ with a Lambda Physik COMPex 102 excimer laser operated as an ArF laser producing 193 nm radiation pulses with fwhm of 25 ns. PH$_2$ was detected by the LIF technique using a Quanta Ray model PDL1 dye laser pumped by a Quanta Ray model DCR1A Nd:YAG laser. The PH$_3$ fragmentation and PH$_2$ laser excitation processes occurred in an anodized Al reaction cell of ca. 750 cm^3 equipped with lateral arms for entrance and exit of the lasers. The axes of the two laser beams were at right angles to each other.

ArF laser energy of 18 mJ/pulse was used.

Deactivation of PH$_2$(Ã^{2}A$_1$) $v_2' = 1$ and $v_2' = 0$ was studied by monitoring the fluorescence time-resolved decay of these species at different pressures of the quenchers. $v_2' = 1$ was generated by excitation of the $^RQ_0(6_{16}-6_{06}$ and $4_{14}-4_{04})$ rotational transitions of the PH$_2$(Ã^{2}A$_1$; $v_2' = 1 - $X̃^{2}B$_1$; $v_2'' = 1$) system with the 551.33 nm laser wavelength, while excitation of $^RQ_0(7_{17}-7_{07}$ and $4_{14}-4_{04})$ of ($v_2' = 0 - v_2'' = 0$) with 546.81 nm radiation was used to produce $v_2' = 0$. The line width and pulse width of the dye laser are 0.3 cm^{-1} and $\cong$5 ns, respectively.

For the quenching of $v_2' = 1$, an Oriel model 77250 $^1/_8$ m low-resolution monochromator was used. The wavelength counter of the monochromator and its slit widths were set at 590.5 nm and 1 mm, respectively. With a fwhm bandpass of 6.4 nm thus obtained, fluorescence from the $v_2' = 1 \rightarrow v_2'' = $

* E-mail : Chieu.NguyenXuan@imip.cnr.it. Telephone: +39-0690672-217, -243. Fax : +39-0690672238.

2 band was selectively recorded. For $v_2'=0$, a Schott OG590 color glass filter allowed the fluorescence due to ($v_2'=0 \rightarrow v_2''=1,2,3,...$) to be monitored.

The fluorescence signals were collected by a 9816 QB Thorn EMI photomultiplier and time analyzed by a 7912AD Tektronix transient digitizer.

Vibrational relaxation of PH$_2$(X̃^{2}B$_1$; $v_2''=1$) and removal of ($v_2''=0$) studies consisted in monitoring the time variation of the concentration of these species and were carried out by excitation of $v_2''=1$ to $v_2'=1$ and $v_2''=0$ to $v_2'=0$ and by collecting the fluorescence signals from $v_2'=1$ and from $v_2'=0$ with the same procedures as above for the quenching studies of $v_2'=1$ and $v_2'=0$. Here, however, the fluorescence was not time analyzed but was time integrated. Time variation was governed by a system of two delay generators, which regulate the time intervals between the photolysis ArF laser flash and the LIF dye laser flash.

The lasers, delay generators, and digitizer were under computer control.

Care was taken to avoid possible contamination of LIF signals with PH$_2$(Ã^{2}A$_1$) fluorescence directly produced in the photolysis of PH$_3$, especially for the time-resolved decay signals, by selecting adequately the time delays between the ArF and dye laser triggerings.

All experiments were performed at room temperature (298 K).

Mixtures of PH$_3$, added gases, and argon buffer gas were supplied to the reaction cell in a slow flow regime by a system of MKS models 147, 250, and 1259 mass flow controllers provided with pressure feedback from capacitance manometers. All experiments were carried out with 0.1 Torr PH$_3$ and 1 Torr argon partial pressures.

As PH$_3$ is a highly toxic gas, the whole experimental apparatus was carefully and frequently leak tested, in particular, a leak test of the gas manifold was performed at every change of gas cylinders. The room was under constant forced ventilation. The quantity of PH$_3$ used was, however, well below the threshold limit value.[8]

The different quenchers with the indicated purity grades were supplied as follows: H$_2$S (99.5%) by Air Liquide, NH$_3$ (99.9990%) by Praxair, COS (99.9%) by Intergas, CHCl$_3$ (99.9%) by Aldrich, and CH$_4$ (99.9995%) by Rivoira.

3. Results and Discussion

3.1. Quenching of PH$_2$(Ã^{2}A$_1$; $v_2'=1$ and 0). Photolysis of PH$_3$ by ArF laser gives rise to formation of both ground (X̃^{2}B$_1$) and excited (Ã^{2}A$_1$) electronic states of PH$_2$. Thus, practically, the collisional deactivation of PH$_2$(Ã^{2}A$_1$) can be studied by monitoring directly its fluorescence decay produced in the photolysis process. However, for reasons of better selectivity of single vibrational levels of Ã^{2}A$_1$, the LIF technique was preferred.

As has been shown in various previous papers,[2] the time decay of the fluorescence signals, from both $v_2'=1$ and $v_2'=0$ of Ã^{2}A$_1$, and in the presence of all the different quenchers dealt with in this work, i.e., H$_2$S, NH$_3$, COS, CHCl$_3$, and CH$_4$, shows a single-exponential trend with decay rate τ^{-1} expressed by:

$$\tau^{-1} = \tau_R^{-1} + k_D + k_{PH3}[PH_3] + k_{Ar}[Ar] + k_M[M] \quad (1)$$

where τ_R is the radiative lifetime of the excited species, k_D their diffusion constant out of the viewing zone, k_{PH3}, k_{Ar}, and k_M
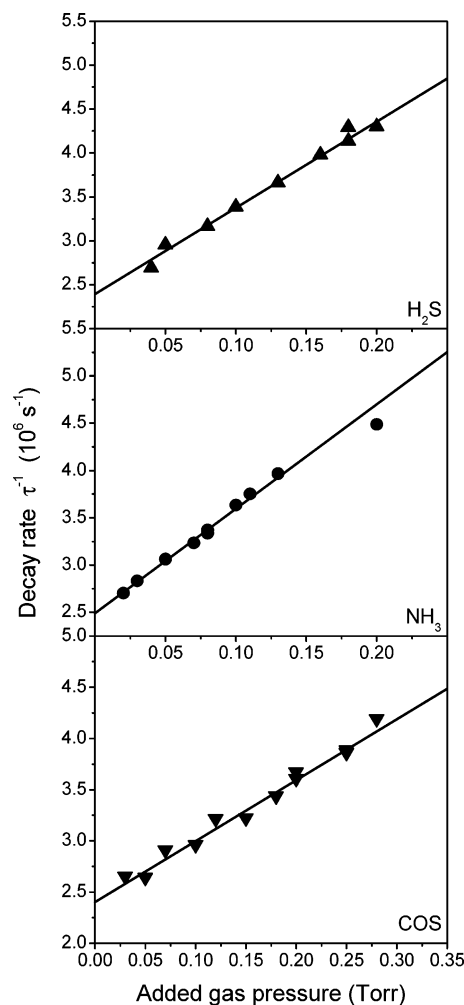

Figure 1. Quenching of PH$_2$(Ã^{2}A$_1$; $v_2'=1$) by H$_2$S, NH$_3$, and COS. Plots of τ^{-1} vs quencher pressure. Mixtures with 0.1 Torr PH$_3$ and 1 Torr Ar.

their quenching constants due to PH$_3$, Ar, and the added gas M, respectively.

τ^{-1} is derived from the slopes of the ln of fluorescence intensities vs time.

Figures 1 and 2 show plots of τ^{-1} against the H$_2$S, NH$_3$, COS, CHCl$_3$, and CH$_4$ pressures for PH$_2$(Ã^{2}A$_1$; $v_2'=1$). Linear least-squares fitting of these plots give the quenching constants due to these molecules: $k_{H2S}=(3.03\pm0.24)$, $k_{NH3}=(3.41\pm0.21)$, $k_{COS}=(1.84\pm0.18)$, and $k_{CHCl3}=(1.98\pm0.18)\times10^{-10}$ cm^3 molec^{-1} s^{-1}, and $k_{CH4}=(5.76\pm0.33)\times10^{-11}$ cm^3 molec^{-1} s^{-1}. Plots of τ^{-1} vs pressures of the same quenchers for (Ã^{2}A$_1$; $v_2'=0$) are shown in Figures 3 and 4, and again, the least-squares fittings give the following quenching constants: $k_{H2S}=(1.72\pm0.14)$ and $k_{NH3}=(1.80\pm0.13)\times10^{-10}$ cm^3 molec^{-1} s^{-1}, and $k_{COS}=(8.20\pm0.34)$, $k_{CHCl3}=(4.98\pm0.31)$, and $k_{CH4}=(2.65\pm0.22)\times10^{-11}$ cm^3 molec^{-1} s^{-1}.

The mathematical treatment of the fluorescence curves and the fitting of plots of τ^{-1} vs [M] pressures have been illustrated extensively in previous papers and, in particular, in ref 9. Briefly, we proceeded in least-squares fitting of the ln values of fluorescence intensities weighted according to Poisson statistics against time to obtain τ^{-1} together with their standard deviations. The different k_M quenching constants and the respective uncertainties were then derived by least-squares fitting of τ^{-1} weighted by their standard deviations against the quencher pressures and also for the calculation of the uncertainties by taking into account the Student's t factor for each plot.
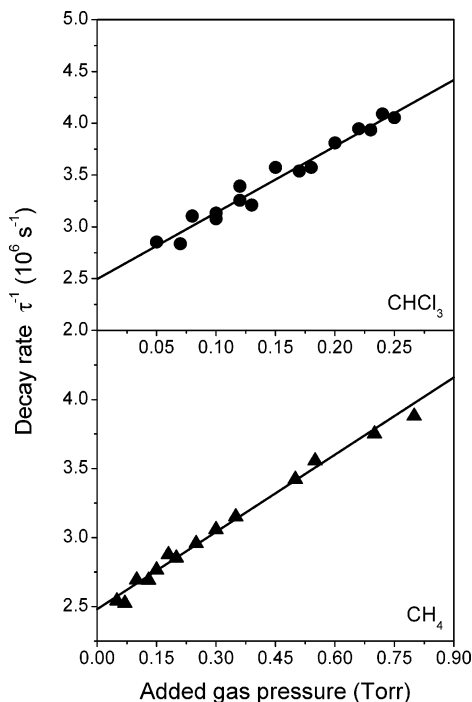
Figure 2. Quenching of $PH_2(\tilde{A}^2A_1; v_2' = 1)$ by $CHCl_3$ and CH_4. Plots of τ^{-1} vs quencher pressure. Mixtures with 0.1 Torr PH_3 and 1 Torr Ar.

In Table 1, the $PH_2(\tilde{A}^2A_1; v_2' = 1$ and 0) quenching constants by the molecules investigated in this work are shown together with the constants due to all of the other molecules already studied in this laboratory.

3.1.a. Parmenter and Co-workers' Model. The quenching data of $PH_2(\tilde{A}^2A_1; v_2' = 1)$ by rare gases have been seen to follow very well the Parmenter et al.'s theory,[6] according to which:

$$\ln \sigma = \beta(\epsilon_{MM}/k)^{1/2} + \ln C \qquad (2)$$

where σ is the cross-section derived from k_M, ϵ_{MM} is the intermolecular well depth of the quenching molecule M, $\beta = (\epsilon_{A*A*}'/kT^2)^{1/2}$ with ϵ_{A*A*}' related to the well depth of the potential between two excited molecules A*, i.e., $PH_2(\tilde{A}^2A_1; v_2' = 1)$, by $(\epsilon_{A*A*})^{1/2} = 0.6(\epsilon_{A*A*}')^{1/2}$. k is the Boltzmann constant, T the temperature, and C a constant.

From the data due to rare gases, $(\epsilon_{PH2*PH2*})/k = 673.1$ K has been obtained and reported in ref 6.

Figure 5 represents $\ln \sigma$ of data reported in Table 1 for $v_2' = 1$ against $(\epsilon_{MM}/k)^{1/2}$, the values of which can be deduced from Table 2. As can be seen, the rare gas data lie on a straight line represented by:

$$\ln \sigma = 0.145(\epsilon_{MM}/k)^{1/2} + 0.162 \qquad (3)$$

Most of the molecular quenchers, however, deviate from this behavior, and attempts to explain these deviations have been made for a certain number of these molecules.[2,12]

The data obtained with the new quenchers of this work seem to allow a better insight into the quenching of $PH_2(\tilde{A}^2A_1)$.

Figure 6 plots $\ln \sigma$ of $PH_2(\tilde{A}^2A_1)$ quenching due to all the molecules so far studied against $(\epsilon_{MM}/k)^{1/2}$ for both $v_2' = 1$ and $v_2' = 0$.

The parallelism between the $v_2' = 1$ and $v_2' = 0$ sets of data has been observed in the previous works,[2] and no more doubt can now be raised about it with the contribution of the new data due to H_2S, NH_3, COS, $CHCl_3$, and CH_4. This parallelism
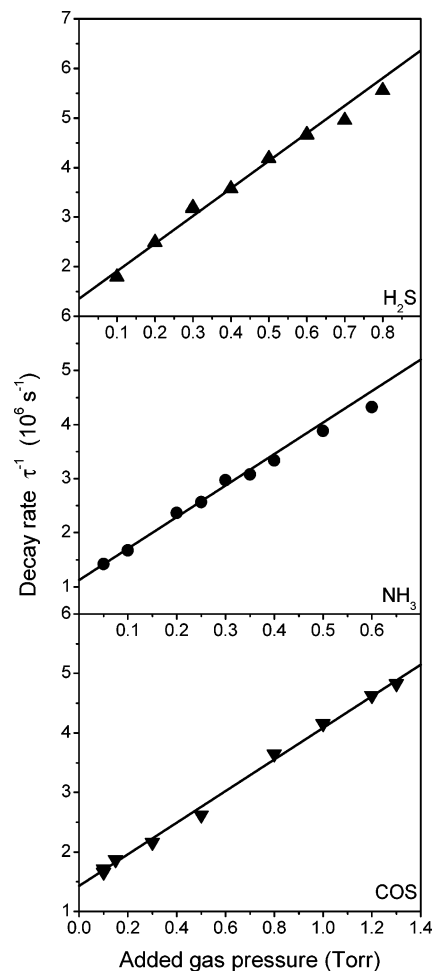

Figure 3. Quenching of $PH_2(\tilde{A}^2A_1; v_2' = 0)$ by H_2S, NH_3, and COS. Plots of τ^{-1} vs quencher pressure. Mixtures with 0.1 Torr PH_3 and 1 Torr Ar.

of sets of data obtained in completely independent experiments is evidence of the fact that their different deviations from the rare gas trend are real, not due to possible experimental fluctuations, and depend only on the different characteristics of the quenchers.

Interesting information can be drawn from Figures 5 and 6.

The polyatomic molecule CH_4, like the diatomic H_2, lies right on the straight line of the rare gas atomic quenchers of Figure 5. Presumably, by virtue of the aforementioned parallelism between $v_2' = 1$ and $v_2' = 0$ quenching data, CH_4 also lies on the rare gas quenching data line of $PH_2(\tilde{A}^2A_1, v_2' = 0)$, which even if not experimentally determined can now be defined by the CH_4 data and the H_2 data already determined in ref 12.

Thus CH_4 should behave as the rare gases in the interaction with $PH_2(\tilde{A}^2A_1)$.

This rare-gas-like behavior of CH_4 will also allow interpretation of the relaxation data of $PH_2(\tilde{X}^2B_1; v_2'' = 1)$ due to this molecule in a later section.

The rare gases can be considered as representing the pure case of collision-induced long-range deactivation of $v_2' = 1$ and $v_2' = 0$ with transition to the isoenergetic higher vibrational level manifold of the $\tilde{X}^2B_1$ ground electronic state. The parallelism of the two $v_2' = 1$ and $v_2' = 0$ quenching data sets is evidence that the rare gas quenching mechanism is present in all of the molecular quenchers so far studied. As has been discussed in ref 12, the difference between the quenching efficiencies of $v_2' = 1$ and $v_2' = 0$ due to the same rare gas

TABLE 1: Quenching of PH$_2$(Ã^{2}A$_1$; $v_2' = 1$ and 0) by Polyatomic^a, Diatomic Molecules, and Rare Gases^b

quencher M	$k_M \times 10^{11c}$ (cm^3 molec^{-1} s^{-1})		σ^d (Å^2)		$P = \sigma/\sigma_{hs}{}^e \times 10^2$	
	$v_2' = 1$	$v_2' = 0$	$v_2' = 1$	$v_2' = 0$	$v_2' = 1$	$v_2' = 0$
H$_2$S	30.3 ± 2.4	17.2 ± 1.4	49.4 ± 3.9	28.0 ± 2.3	122	69.0
NH$_3$	34.1 ± 2.1	18.0 ± 1.3	45.4 ± 2.8	24.0 ± 1.8	127	67.2
COS	18.4 ± 1.8	8.20 ± 0.34	33.7 ± 3.2	15.1 ± 0.6	72.1	32.2
CHCl$_3$	19.8 ± 1.8	4.98 ± 0.31	40.0 ± 3.7	10.1 ± 0.6	62.7	15.8
CH$_4$	5.76 ± 0.33	2.65 ± 0.22	7.53 ± 0.43	3.47 ± 0.29	17.5	8.1
CO$_2$	8.64 ± 0.43	2.96 ± 0.12	14.9 ± 0.7	5.12 ± 0.21	33.0	11.3
N$_2$O	9.07 ± 0.36	2.98 ± 0.11	15.7 ± 0.6	5.16 ± 0.19	35.8	11.8
SO$_2$	22.0 ± 2.9		40.9 ± 5.5		83.8	
PH$_3$	34.4 ± 3.3	24 ± 5	56.0 ± 5.4	39 ± 8	134	95
H$_2$	5.79 ± 0.44	2.60 ± 0.10	3.17 ± 0.24	1.42 ± 0.03	9.50	4.28
N$_2$	5.05 ± 0.39	2.12 ± 0.10	7.82 ± 0.61	3.28 ± 0.11	18.8	7.90
CO	7.40 ± 0.62	3.44 ± 0.18	11.5 ± 1.0	5.33 ± 0.27	28.3	13.2
NO	19.6 ± 1.8	7.70 ± 0.35	30.9 ± 2.9	12.1 ± 0.6	78.2	30.8
He	2.51 ± 0.22		1.88 ± 0.17		6.3	
Ne	2.03 ± 0.18		2.86 ± 0.25		8.9	
Ar	3.24 ± 0.11		5.49 ± 0.18		14.3	
Kr	3.78 ± 0.14		7.32 ± 0.27		18.0	
Xe	5.50 ± 0.41		11.2 ± 0.8		24.2	

^{a} The data by H$_2$S, NH$_3$, COS, CHCl$_3$, and CH$_4$ have been obtained in this work. The other data come from previous studies (see ref 2). ^{b} Rate constants k_M, cross sections σ, and probability per collision P. ^{c} The data are reported with 95% confidence level errors. ^{d} The cross sections have been derived from k_M using the formula reported in ref 10, pp 16−19. ^{e} To calculate the various hard sphere collision cross-sections σ_{hs}, the diameter of PH$_2$ has been estimated as approximately equal to that of H$_2$S (see ref 11).
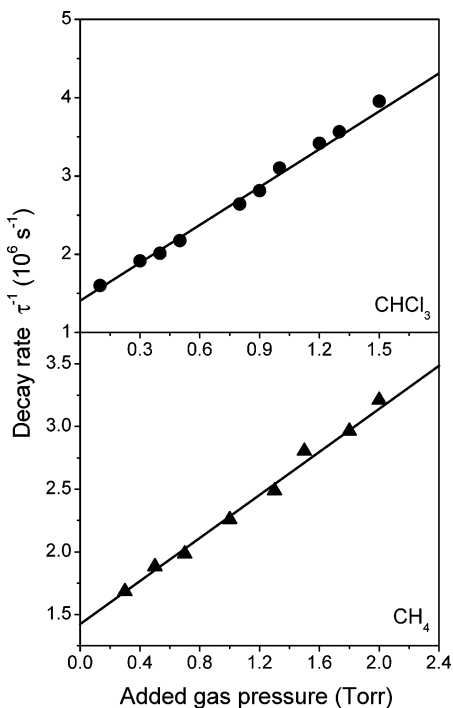

Figure 4. Quenching of PH$_2$(Ã^{2}A$_1$; $v_2' = 0$) by CHCl$_3$ and CH$_4$. Plots of τ^{-1} vs quencher pressure. Mixtures with 0.1 Torr PH$_3$ and 1 Torr Ar.

should be governed by the difference in density of states of the PH$_2$ ground electronic state underlying $v_2' = 1$ and $v_2' = 0$.

The higher quenching values by most of the molecular quenchers with respect to what was expected from the rare gas eq 3 thus must be due to additional mechanisms.

In ref 12, the difference in PH$_2$(Ã^{2}A$_1$; $v_2' = 1$) quenching efficiencies of H$_2$, N$_2$, CO, and NO has been tentatively first ascribed to an intermolecular V−V process resulting in a (Ã^{2}A$_1$; $v_2' = 1 \rightarrow v_2' = 0$) vibrational relaxation. The increase of quenching constants going from H$_2$ to NO should be due to decrease in energy gap between the vibrational relaxation energy ($v_2' = 1 - v_2' = 0$: 951.3 cm^{-1}) and the vibrational frequencies of the diatomic molecules (4401, 2359, 2170, and 1904 cm^{-1}
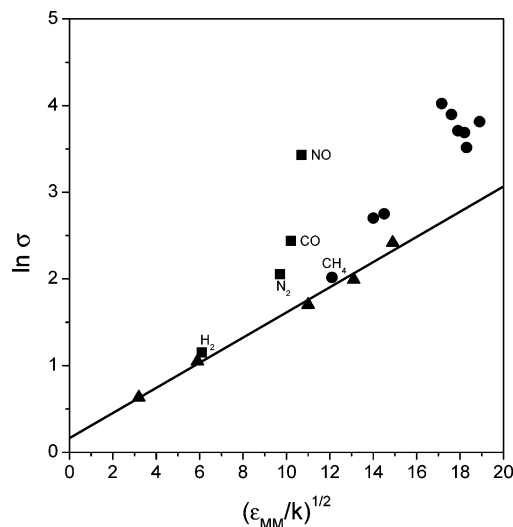

Figure 5. Parmenter's plot for PH$_2$(Ã^{2}A$_1$; $v_2' = 1$) quenching by: (▲) rare gases; (■) diatomic molecules: H$_2$, N$_2$, CO, and NO; (●) polyatomic molecules. Solid line from rare gas data fit.

for H$_2$, N$_2$, CO, and NO, respectively). The same trend, however, has also been observed, as shown in Figure 6, for PH$_2$(Ã^{2}A$_1$; $v_2' = 0$) quenching, which should decay with the same mechanisms of $v_2' = 1$, but for which a vibrational relaxation process cannot be contemplated. On the other hand, due to the high values of the above-mentioned energy gaps, the probability of a V−V process for $v_2' = 1$ should be very low and should not be able to justify the values of the deviations from the rare gas trend.

An intermolecular E−V process has then been proposed in which part of the vibronic energy of PH$_2$(Ã^{2}A$_1$; $v_2' = 1$ or 0) is transferred to the vibrations of the diatomic quenchers and $v_2' = 1$ or 0 is deactivated to some lower vibrational levels of the ground electronic state. The efficiency of the process should increase with the decrease of the quencher vibration frequency, and this should account for the trend shown by H$_2$, N$_2$, CO, and NO. However, in light of the CH$_4$ data gathered in the present work, this mechanism could not be accepted either. In fact, if it is operative, CH$_4$ would be more efficient than N$_2$ and CO in quenching PH$_2$(Ã^{2}A$_1$; v_2'), as it has the frequencies

TABLE 2: Selected Molecular Properties[a] of PH$_2$ and the Investigated Quenchers, and Calculated Quenching Cross Sections σ_{calc} according to Collision Complex Model

PH$_2$ and quencher M	d_M (Å)	D_M (Debye)	q_M (Å^2)	α_M (Å^3)	ϵ_{MM}/k (K)	I_M (eV)	σ_{calc} (Å^2)
PH$_2$	3.591	0.574	0.21	2.85	139.3	7.55	
H$_2$S	3.591	0.973	0.218	3.78	309	10.453	101
NH$_3$	3.15	1.47	0.208	2.26	357.2	10.19	105
COS	4.13	0.712	0.60	5.7	334.9	11.1	110
CHCl$_3$	5.430	1.01	0.80	8.66	331.2	11.4	129
CH$_4$	3.80	0	0	2.6	146.4	12.71	68
SO$_2$	4.29	1.63	0.92	4.28	320.4	12.3	128
N$_2$O	3.879	0.167	0.687	3.03	210.3	12.89	86
CO$_2$	4.00	0	0.897	2.91	196.0	13.77	85
PH$_3$	3.5	0.574	0.436	4.27	294	9.87	97
H$_2$	3.0	0	0.14	0.79	37.2	15.4	50
N$_2$	3.7	0	0.29	1.76	94.1	15.6	66
CO	3.6	0.112	0.33	1.95	104.0	14.0	71
NO	3.5	0.153	0.29	1.74	114.5	9.25	67
He	2.6	0	0	0.204	10.2	24.6	31
Ne	2.8	0	0	0.393	34.8	21.6	38
Ar	3.4	0	0	1.66	121.0	15.7	60
Kr	3.6	0	0	2.48	171.6	14.0	68
Xe	4.1	0	0	4.00	222.0	12.1	78

[a] Diameter (d_M), dipole moment (D_M), quadrupole moment (q_M), polarizability (α_M), potential well depth (ϵ_{MM}/k), ionization potential (I_M). The molecular properties are selected from refs 1−5, 9, 13−19. The quadrupole moment of H$_2$S has been taken from ref 19. For CHCl$_3$, we have assumed the value of the quadrupole moment of CHF$_3$ reported in ref 15, as quadrupole moments for other similar molecules are not available.
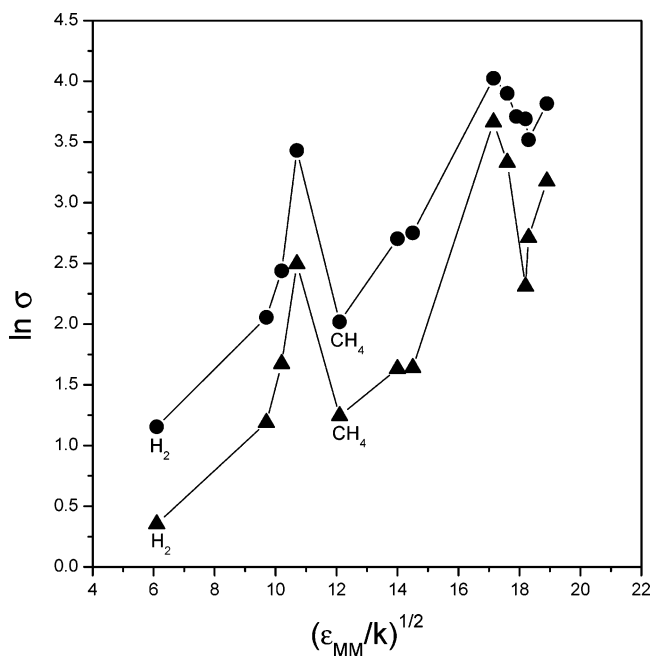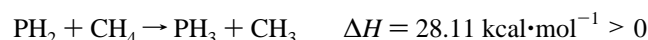

Figure 6. Parmenter's plot for PH$_2$($\tilde{A}^2A_1$; $v_2' = 1$ and 0) quenching by diatomic and polyatomic quenchers: (●) $v_2' = 1$ data, (▲) $v_2' = 0$ data.

of two normal vibration modes far lower than those of these two molecules.

As recalled in the Introduction of this paper, in the case of NO, it is known that this molecule gives rise to chemical reaction with ground PH$_2$($\tilde{X}^2B_1$).[7] Thus it is presumable that PH$_2$($\tilde{A}^2A_1$; v_2') is removed not only by collisions with NO but also by chemical reaction, which constitutes then the additional de-activation channel.

As will be illustrated in a later section, experiments of interaction between PH$_2$($\tilde{X}^2B_1$; $v_2'' = 0$) and all of the quenchers treated in this work have been carried out, but no chemical reactions have been revealed. Here, however, we are dealing with interactions of these molecules with PH$_2$($\tilde{A}^2A_1$; $v_2' = 1$ and $v_2' = 0$), i.e., in a different energetic context where the occurrence of reactions could be possible. The lack of knowl-edge about the nature of possible reactions,

however, hinders an estimation of their occurrence from the thermodynamic point of view. We have tried to figure out some simple reactions and calculate the reaction enthalpies of ground state reactants that result in being all endothermic and confirm the above-mentioned nonreaction experimental results. These endothermic enthalpies could, however, be overcome by the vibronic energy of PH$_2$($\tilde{A}^2A_1$; $v_2' = 1$) and PH$_2$($\tilde{A}^2A_1$; $v_2' = 0$), which are 55.0 and 52.3 kcal/mol, respectively. This, however, means only that these reactions are energetically permitted, while whether the reactions do occur or not is another question. In fact, the simplest reactions between H$_2$ and CH$_4$ with ground state PH$_2$ are:

$$PH_2 + H_2 \rightarrow PH_3 + H \qquad \Delta H = 27.5 \text{ kcal·mol}^{-1} > 0$$

$$PH_2 + CH_4 \rightarrow PH_3 + CH_3 \qquad \Delta H = 28.11 \text{ kcal·mol}^{-1} > 0$$

respectively. These reactions thus are endothermic. By adding the vibronic energy of 55.0 kcal·mol^{-1} ($\tilde{A}^2A_1$; $v_2' = 1$) or 52.3 kcal·mol^{-1} ($\tilde{A}^2A_1$; $v_2' = 0$) to the energy content of PH$_2$, the above ΔH values turn negative and the reactions become exothermic. The rare-gas-like behavior, as it appears in Figure 5, of H$_2$ and CH$_4$, however, shows that their interactions with PH$_2$($\tilde{A}^2A_1$; v_2') do not give rise to chemical reactions.

In the Parmenter et al.'s theory and in the following collision complex model, the formation of an intermediate complex before the deactivation of the excited species by the quenching molecule is considered. As the molecular properties, dipole and quadrupole moments, and polarizabilities are different for different quenchers (see Table 2), it is obvious that the collision complex is more or less tightly bound and then has a lifetime that varies with the nature of the quenching molecule. The longer the lifetime is, the longer the contact between the excited molecule and the quencher is and then the higher the probability of energy randomization becomes, leading to a higher probability of deactivation of the excited species. In the cases of N$_2$ and CO, if no reactions can occur, the presumably more tightly bound collision complex with respect to that of CH$_4$ could explain their higher quenching efficiencies. It is to be noted that the above-mentioned chemical reactions should also occur via a collision complex, which could lead to the formation of an intermediate adduct before the formation of products.
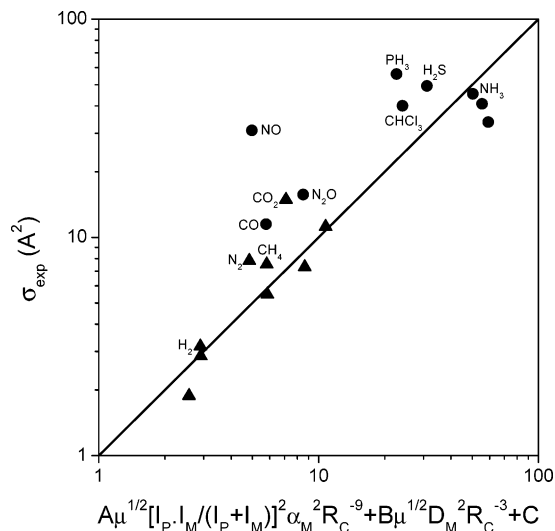
Figure 7. Thayer and Yardley's plot for the quenching of PH$_2$(Ã^{2}A$_1$; v_2' = 1) by: (▲) rare gases and nonpolar quenchers, (●) polar quenchers.

The deviations of the molecular quenching constants from the rare gas trend should thus be due to additional quenching channels, which could be chemical reactions and/or more tightly bound collision complexes with longer complex lifetimes and more efficient energy randomization.

In consideration of the parallel variation trends with the quenchers of v_2' = 1 and v_2' = 0, all that has been said above for v_2' = 1 might grosso modo be extended to v_2' = 0.

3.1.b. Thayer and Yardley's Model. Thayer and Yardley[4] based their theory of excited electronic species quenching on the instantaneous dipole–dipole interactions between molecules and worked out the following expressions for the deactivation efficiency:

$$\sigma = A\mu^{1/2}[I_P I_M/(I_P + I_M)]^2\alpha_M^{\,2}R_C^{\,-9} + C \tag{4}$$

for nonpolar quenchers and:

$$\sigma = A\mu^{1/2}[I_P I_M/(I_P + I_M)]^2\alpha_M^{\,2}R_C^{\,-9} + B\mu^{1/2}D_M^{\,2}R_C^{\,-3} + C \tag{5}$$

for polar quenchers, where μ is the reduced mass of the collision pair, I_P the ionization potential of the excited molecule, I_M, α_M, and D_M the ionization potential, polarizability, and dipole moment of the quencher, and R_C the hard sphere distance between the molecules of the collision pair. A and C are the constants to be deduced from data due to nonpolar quenchers according to eq 4. B is obtained from eq 5 for polar quenchers, with A and C derived as above.

Thayer and Yardley's model considers a collision-induced transition of the excited state to a continuum and the Fermi "golden rule" has been used to treat the dipole matrix elements, leading to the above equations.

The fact that the quenching efficiencies due to rare gases follow eq 4 very well is thus evidence of a deactivation of PH$_2$(Ã^{2}A$_1$; v_2' = 1) through transitions to an underlying high-density higher vibrational manifold of the ground electronic state.[6]

Figure 7 represents the plot of experimentally determined quenching cross-sections of PH$_2$(Ã^{2}A$_1$; v_2' = 1) shown in Table 1 against the cross-sections calculated with eq 5, where the second term disappears for nonpolar molecules.

Table 2 reports the molecular properties used for these calculations.

As can be seen, except for the cases of N$_2$ and CO$_2$, all of the nonpolar gases treated follow well the Thayer and Yardley's correlation, while all of the polar quenchers with the exception of NH$_3$ deviate clearly from it. However, if we adopt the criterion of these authors who considered as acceptable a deviation of the experimental data by a factor of $\cong$1.5 from the unity slope straight line,[4] all of the data collected, apart from the clearly anomalous value of NO, on the whole seem to agree with the theory.

It is interesting to see, as we have already observed with the Parmenter et al.'s theory, that also with this theory the two nonpolar molecules N$_2$ and CO$_2$ do not behave like the rest of the nonpolar molecules studied.

3.1.c. Collision Complex Model. For this theory,[5] a complex is formed in the collision of the molecules and a redistribution of the internal energies between the partners occurs before its redissociation, giving rise to the quenching of the excited species. A capture cross-section $\sigma_{cap}(E)$ between the collision partners is then calculated, which represents the maximum cross-section a quenching process could achieve. The actual efficiency should be given by the product of this maximum cross-section and a probability $P(E)$ that the process really occurs. These quantities are functions of the collision kinetic energy E.

$$\sigma(E) = P(E)\cdot\sigma_{cap}(E) \tag{6}$$

In a molecular encounter, the effective potential between the partners is expressed by:

$$V(r) = Eb^2/r_2 - C_3/r_3 - C_4/r_4 - C_6/r_6 - C_6'/r_6 \tag{7}$$

where the first term represents a repulsive centrifugal barrier with b as the impact parameter. The other four terms are the attractive multipole interactions (dipole–dipole, dipole–quadrupole, dipole–induced dipole, and dispersion). The different C functional forms can be found in refs 13 and 20, with multipole orientations chosen for maximum interaction.

For each E and each b, $V(r)$ presents a maximum. Only collisions with E larger than or equal to this maximum can lead to a mutual capturing of the partners and the formation of a complex. A $b_0(E)$ corresponding to this maximum can be deduced, giving:

$$\sigma_{cap}(E) = \pi b_0(E)^2$$

$b_0(E)$ has been calculated by following the approach outlined by Fairchild et al.,[13] which consists in considering the multipole interactions as operative simultaneously and not that of Lee and co-workers,[5] which considers the capture cross-section as due to a sum of partial cross-sections produced by different types of multipole interactions acting independently. For the numerical computation, we have, however, adopted the procedure of Hofzumahaus and Stuhl,[20] which gives the same results as those obtained by the Fairchild et al.'s method. $\sigma_{cap}(E)$ is then derived and thermally averaged, giving the quantity to be compared with the experimental data.

The calculated cross-sections are shown in Table 2, together with the molecular properties.

Figure 8 plots the experimental cross-sections of PH$_2$(Ã^{2}A$_1$; v_2' = 1) quenching against the calculated data.

The nonpolar quenchers, except CO$_2$, are correlated by the least-squares fitting line, while the data due to more polar molecules appear scattered randomly.
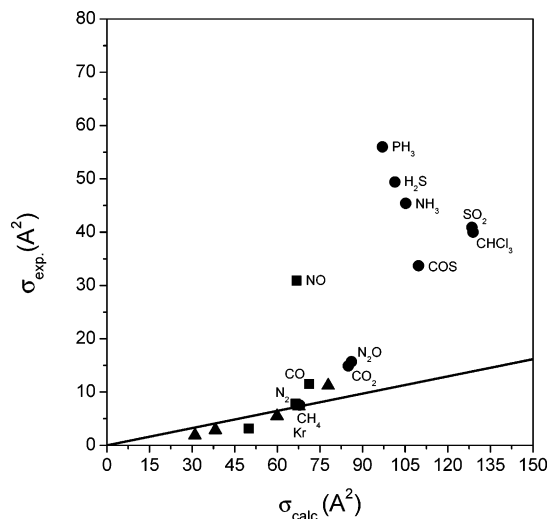
Figure 8. Plot of $PH_2(\tilde{A}^2A_1; v_2' = 1)$ deactivation experimental cross sections vs collision complex theory calculated cross sections: (▲) rare gas quenchers, (■) diatomic molecules, (●) polyatomic molecules. Line: fit of rare gases and H_2, N_2.

In agreement with eq 6, the probability P for the occurrence of the quenching process should be 0.1 for the quenchers lying on the correlation line, i.e., rare gases, H_2, N_2, and CH_4. This value is of the same order of magnitude as those shown in Table 1.

With the molecules studied in this work, we now have available a presumably sufficient number of data to get an idea about the capability of the proposed theories to deal with experimental quenching data of $PH_2(\tilde{A}^2A_1)$.

The main conclusion that can be drawn is that none of these theories has, strictly speaking, succeeded in establishing a relationship between the quenching cross-sections and the molecular properties for the polar quenchers, while they can account fairly well for the data due to rare gases and some nonpolar molecules. For rare gases and these nonpolar molecules, the quenching of $PH_2(\tilde{A}^2A_1; v_2'')$ should be due prevalently to long-range interactions, whereas for the rest of molecular quenchers, the deactivation process could involve additional channels such as chemical reactions and/or higher-efficiency quenching due to the longer lifetime of the intermediate collision complex.

3.2. Vibrational Relaxation of $PH_2(\tilde{X}^2B_1; v_2'' = 1)$. It is known that absorption of ArF laser 193 nm photons by PH_3 produces ground electronic state PH_2 radicals in the excited vibrational levels $v_2'' > 3$ of the bending mode.[21] The reason for this absence of lower vibrational levels is due to the fact that the HPH angle in the planar intermediate excited PH_3* molecule is 114°, while this angle in PH_2 is only 91°42′. The fragmentation of PH_3* then results in the formation of excited PH_2 vibrational species.
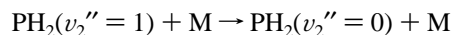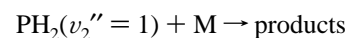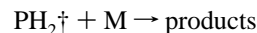
This lack of $v_2'' < 3$ states is further confirmed by the time-resolved LIF curves monitoring the time variation of $PH_2(\tilde{X}^2B_1; v_2'' = 1)$ concentrations. These curves show a build-up and a decay branch and are seen to follow the equation:

$$I(t) = C[-\exp(-Bt) + \exp(-At)] \quad (8)$$

which represents the variation of the population of the lower level of a two-level system coupled to a ground state. This lower level with A as decay constant has zero population at $t = 0$ and is populated by relaxation from the upper one.

A kinetic scheme has been proposed to describe the variation of $PH_2(\tilde{X}^2B_1; v_2'' = 1)$ concentration in terms of different

deactivation constants and also of possible chemical reaction constants.[12] It is here presented in a condensed form:

$$PH_2\dagger + M \rightarrow products$$

$$PH_2\dagger + M \rightarrow PH_2(v_2'' = 1) + M$$

$$PH_2(v_2'' = 1) + M \rightarrow products$$

$$PH_2(v_2'' = 1) + M \rightarrow PH_2(v_2'' = 0) + M$$

where $PH_2\dagger$ represents the higher bending vibrational levels produced by PH_3 photolysis and M, the quenching molecule.

The following expression has been obtained by imposing $[(v_2'' = 1)] = 0$ at $t = 0$:

$$[PH_2(v_2'' = 1)] = \\ [PH_2\dagger]_0\{K/(K2 - K1)\}\{-\exp(-K2t) + \exp(-K1t)\} \quad (9)$$

where K is a constant that takes into account the relaxation of $PH_2\dagger$ to $v_2'' = 1$ due to collisions with M, PH_3, and Ar. $K2$ and $K1$ represent the total decay rates of $PH_2\dagger$ and $v_2'' = 1$, respectively.

As can be seen, eq 9 is of the same functional form as eq 8, so eq 9 should represent the recorded time-resolved LIF curves of $PH_2 (v_2'' = 1)$ population.

The detailed expressions of $K2$ and $K1$ in terms of constants of single reactions can be found in ref 12.

It is here sufficient to know that $K1$, which concerns the species under investigation, i.e., $v_2'' = 1$, can be represented by:

$$K1 = a[M] + b \quad (10)$$

where a is the sum of the collision-induced deactivation constant and the constant of a possible chemical reaction of $v_2'' = 1$ with M, b instead is the sum of all the quenching events due to collisions with the parent molecule PH_3 and the buffer gas Ar and is a constant, as it is the sum of products between the constants of single reactions and the concentrations of PH_3 or Ar.

For all of the quenchers under study, measurements of removal of $PH_2(\tilde{X}^2B_1; v_2'' = 0)$ have also been done by monitoring the time variation of $v_2'' = 0$ concentration at different quencher pressure with the same LIF technique as for $v_2'' = 1$, and by using the $v_2' = 0 - v_2'' = 0$ transition band excitation wavelength of 546.81 nm. The decay rates are of the order of $4-5 \times 10^2$ s^{-1}, i.e., ≈ 2 orders of magnitude lower than the decay rates recorded for removal of $PH_2(\tilde{X}^2B_1; v_2'' = 1)$ and have been seen to either remain approximately constant or even decrease with the increase of the quencher pressure in a pressure range much wider than that operative in the $v_2'' = 1$ relaxation experiments. These results show thus that no chemical reactions have taken place between $PH_2(\tilde{X}^2B_1; v_2'' = 0)$ and the quenching molecules. The decay rates observed are due to diffusion out of the viewing zone and slow gas flows.

Then, a of eq 10 actually represents only the deactivation constant.

In most experimental LIF curves, the build-up branch has poor statistics, so we preferred to treat only the decay branch, sufficiently far away from the maximum in order to reduce eq 9 to:

$$[PH_2(v_2'' = 1)] = [PH_2\dagger]_0\{K/(K2 - K1)\}\cdot\exp(-K1t) \quad (11)$$

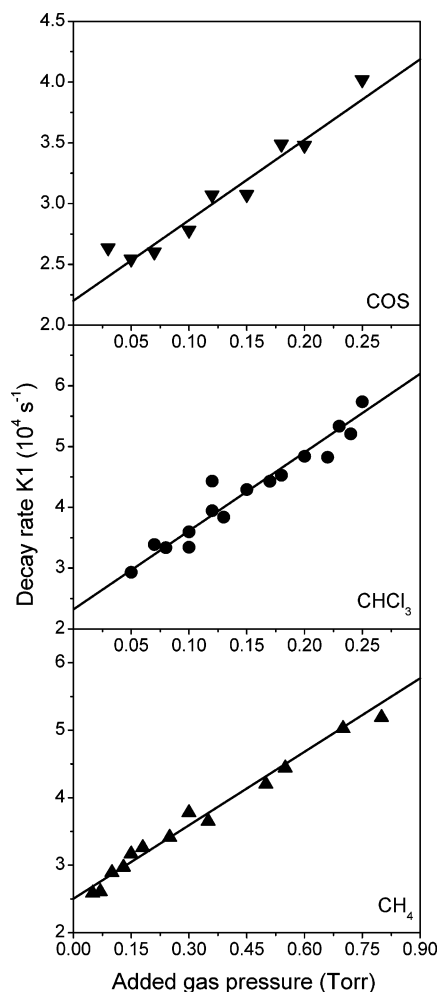**Figure 9.** PH$_2$($\tilde{X}^2B_1$; $v_2'' = 1$) LIF curve decay rate K1 vs pressure of COS, CHCl$_3$, and CH$_4$. Mixtures with 0.1 Torr PH$_3$ and 1 Torr Ar.

Least-squares fitting of ln values of LIF intensities against t gives $K1$.

In Figure 9 , $K1$ is plotted against [M] for COS, CHCl$_3$, and CH$_4$. Weighted least-squares fittings with eq 10 give the deactivation constants of PH$_2$($\tilde{X}^2B_1$; $v_2'' = 1$).

In Table 3, these constants are presented together with all of those determined in previous works in order to give the whole picture of the collision induced PH$_2$($v_2'' = 1$) deactivation data.

By comparison of the deactivation efficiencies by the polyatomic molecules with those due to rare gases and diatomic molecules, it can be inferred that the polyatomic molecules interact with PH$_2$($v_2'' = 1$) through a V$-$V process.

In ref 1, a linear relationship, similar to the Callear's line,[10,22] between the log values of PH$_2$($v_2'' = 1$) deactivation probabilities and the difference in energy $\Delta\nu$ (cm^{-1}) between ($v_2'' = 1$) and the frequency of the energetically closest vibrational mode of the quenching molecule has been observed with SO$_2$, H$_2$S, N$_2$O, and CO$_2$. Measurements have thus been done with other molecules in order to gather more data in the range of $\Delta\nu$ investigated.

In this work, the molecule CHBr$_3$ has also been considered, but the mixture with PH$_3$ under the action of ArF laser gives rise to very fast but unknown reactions that prevent measurements from being carried out.

Table 4 shows the different normal vibrational modes of all the polyatomic quenchers so far studied and the minimum $\Delta\nu$.

Figure 10 plots log P against $\Delta\nu$. The first molecules that have been shown in this plot,[2] i.e., CO$_2$, N$_2$O, SO$_2$, and PH$_3$,

TABLE 3: Collision-Induced Removal of PH$_2$($\tilde{X}^2B_1$; $v_2'' = 1$)^a

quencher M	$\mu^{1/2}$	$k_M \times 10^{14b}$ (cm^3 molec^{-1} s^{-1})	$\sigma \times 10^3$ (Å^2)	$P = \sigma/\sigma_{hs} \times 10^4$
CHCl$_3$	5.08	399 ± 66	807 ± 133	126 ± 21
COS	4.61	204 ± 34	375 ± 62	80.1 ± 13.2
H$_2$S	4.09	191 ± 18	311 ± 30	76.7 ± 7.4
NH$_3$	3.35	614 ± 59	819 ± 79	229 ± 22
CH$_4$	3.28	112 ± 12	146 ± 16	34.1 ± 3.7
SO$_2$	4.67	189 ± 42	350 ± 79	71.9 ± 16.2
CO$_2$	4.34	54.4 ± 6.6	94.0 ± 11.5	20.8 ± 2.5
N$_2$O	4.34	119 ± 11	206 ± 19	47.1 ± 4.3
PH$_3$	4.09	456 ± 37	743 ± 60	188 ± 15
NO	3.96	668 ± 157	1054 ± 248	269 ± 63
CO	3.89	15.9 ± 2.1	24.6 ± 3.2	6.1 ± 0.8
N$_2$	3.89	5.09 ± 0.44	7.89 ± 0.69	1.9 ± 0.2
H$_2$	1.38	58.4 ± 12	32.0 ± 6.4	9.6 ± 1.9
Kr	4.87	7.65 ± 1.71	14.8 ± 3.3	3.65 ± 0.8
Ar	4.25	6.70 ± 1.37	11.3 ± 2.3	2.95 ± 0.6
Ne	3.54	6.26 ± 0.70	8.82 ± 0.99	2.75 ± 0.3
He	1.89	9.77 ± 1.66	7.34 ± 1.24	2.44 ± 0.4

^{a} The data for COS, CHCl$_3$, and CH$_4$ are obtained in this work while those of the other quenchers come from previous papers (see refs 1 and 2). Reduced mass of the collision pair $\mu^{1/2}$, rate constants k_M, cross-sections σ, and probabilities per collision P. The cross-sections have been derived from k_M using the formula given in Yardley, J. T., ref 10, pp 16$-$19. The room temperature is 298 K. ^{b}Confidence level errors of 95% are reported.

give rise to endothermic V$-$V processes. Thus, to be reported on the same plot, the data of molecules, such as NH$_3$ and COS, which produce exothermic reactions, have to be converted to endothermic data through the principle of detailed balance.

The molecules SO$_2$, H$_2$S, N$_2$O, COS, CO$_2$, and CH$_4$ lie on a straight line, while PH$_3$, NH$_3$, and CHCl$_3$ clearly deviate from it.

In ref 1, it has been demonstrated that the behavior of NH$_3$ is due to the inversion doubling of this molecule. NH$_3$ is known to have a pyramidal geometry with the N atom on top of the structure. The nitrogen atom, besides its participation in the normal vibrations of the molecule, can undergo a so-called flip$-$flop movement, which brings it back and forth from one side to the other of the H$_3$ plane. This movement causes a splitting of the vibrational levels of ν_2, which is the mode interacting with PH$_2$($v_2'' = 1$), into two sets of symmetric and antisymmetric levels, in particular, $\nu_2 = 0$ becomes $\nu_2 = 0^+$(s) and $\nu_2 = 0^-$(a). Thus, in the collision complex, PH$_2$($v_2'' = 1$) should be in contact with both of these levels and then can release its energy to both of them. The energy levels of the symmetric and antisymmetric systems are slightly different, then the $\Delta\nu$ should be different depending on the symmetry state of NH$_3$ $\nu_2 = 0$ levels with which V$-$V exchange of PH$_2$($v_2'' = 1$) occurs. These two $\Delta\nu$ quantities are known, then from the line of Figure 10, the corresponding deactivation probabilities can be deduced, and in fact, their sum has been found to agree very well with the experimental global probability. More simply, we can also say that, because of this inversion of NH$_3$, the probability of deactivation of PH$_2$($v_2'' = 1$) is doubled. Effectively, if we divide by 2 the experimental probability, we obtain data, represented by the △ (upward open triangle) symbol, which agrees very well with the line of Figure 10. The linear relationship log $P - \Delta\nu$ should thus also be valid for NH$_3$ if this molecule does not undergo inversion.

The effect of inversion in NH$_3$ has been well-known in absorption spectroscopy with the detection of line doubling since the 1940s. To our knowledge, it is here pointed out for the first time the influence of NH$_3$ inversion in an energy transfer process.

TABLE 4: Normal Vibration Frequencies of PH$_2$($\tilde{X}^2B_1$) and the Polyatomic Quenchers^a under Study; Minimum Frequency Mismatch $\nu_{PH2}-\nu_n$ between the Vibrations of PH$_2$ and the Quenchers.

	ν_1 (cm^{-1})	ν_2 (cm^{-1})	ν_3 (cm^{-1})	ν_4 (cm^{-1})	$\Delta\nu = \nu_{PH2} - \nu_n$ (cm^{-1})	$P = \sigma/\sigma_{hs} \times 10^4$
PH$_2$		1102				
COS	2062	520	859		+243 ($n = 3$)	80.1 ± 13.2
CHCl$_3{}^b$	3034	680	363	1220	−118 ($n = 4$)	126 ± 21
CH$_4$	2917	1534	3019	1306	−204 ($n = 4$)	34.1 ± 3.7
H$_2$S	2614.6	1182.7	2627.5		−80.7 ($n = 2$)	76.7 ± 7.4
NH$_3$	3337	950	3444	1627	+152 ($n = 2$)	229 ± 22
PH$_3$	2322.9	992.0	2327.7	1122.4	−20.4 ($n = 4$)	188 ± 15
SO$_2$	1151.3	517.6	1361.7		−49.3 ($n = 1$)	71.9 ± 16.2
N$_2$O	2223.8	588.8	1284.9		−182.9 ($n = 3$)	47.1 ± 4.3
CO$_2$	1388.2	667.4	2349.2		−286.2 ($n = 1$)	20.8 ± 2.5

^{a} The normal vibration frequencies are taken from refs 23 and 24. ^{b} For CHCl$_3$, ν_5 and ν_6 have not been shown because, having frequencies of 774 and 261 cm^{-1}, respectively, they would not participate, like ν_1, ν_2, and ν_3, in the V−V process with PH$_2$($\tilde{X}^2B_1$; $\nu_2'' = 1$).
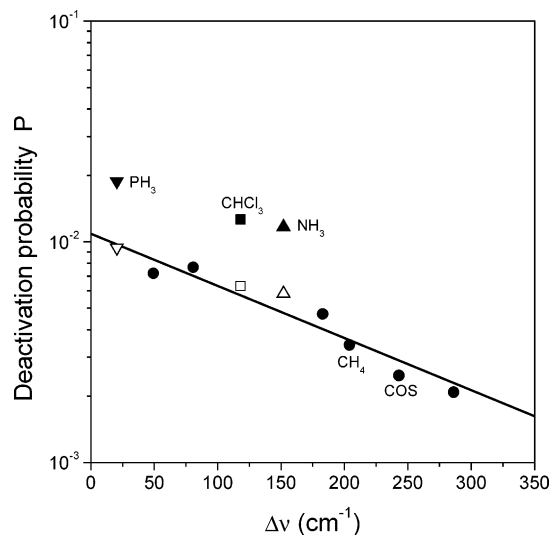

Figure 10. Deactivation probability of PH$_2$($\tilde{X}^2B_1$; $\nu_2'' = 1$) vs $\Delta\nu$. Solid symbols: experimental data. Open symbols: data of corresponding solid symbols divided by 2, see text. (●) data of SO$_2$, H$_2$S, N$_2$O, CH$_4$, COS, and CO$_2$, Line: fit of SO$_2$, H$_2$S, N$_2$O, and CO$_2$ data.

The explanation for the high value of quenching efficiency by CHCl$_3$ with respect to that expected from the straight line of Figure 10 has to be of a different nature.

An examination of the symmetry species of the normal vibrations of the quenchers^{24} so far dealt with shows that the vibrations, involved in V−V energy exchange with PH$_2$($\nu_2'' = 1$) (Table 4), of the molecules, which are correlated by the line in Figure 10, are all nondegenerate vibrations.

ν_4 of CHCl$_3$ responsible for the de-excitation PH$_2$($\nu_2'' = 1$) instead is an e symmetry species, i.e., has a two-dimensional symmetry representation. This means that ν_4 of CHCl$_3$ is doubly degenerate. CHCl$_3$ thus has two normal vibrational modes with the same frequency ν_4 interacting with PH$_2$($\nu_2'' = 1$), which can then release its excitation energy to both $\nu_4 = 0$ levels of the two ν_4 degenerate modes of the quencher. The deactivation efficiency of PH$_2$($\nu_2'' = 1$) should then be twice that expected from the line of Figure 10 in the case where ν_4 is a nondegenerate vibration. In fact, by dividing by 2 the experimental data, we obtain a point, represented by the □ (open square) symbol, which correlates well with the other quenchers of the line.

To our knowledge, this is also the first time that the effect of the degenerate vibrations has been experimentally demonstrated.

In ref 1, the quenching efficiency due to PH$_3$ is interpreted as the sum of transfer probabilities of PH$_2$($\nu_2'' = 1$) energy to both ν_4 and ν_2 vibrational modes of PH$_3$, with $P_{\nu4} = 9.73 \times 10^{-3}$ ($\Delta\nu = -20.4$ cm^{-1}) and $P_{\nu2} = 9.07 \times 10^{-3}$ ($\Delta\nu = +110$ cm^{-1}). But in light of what has just been discovered about the

effect of the degenerate vibrations of the quencher on the efficiency of energy exchange, this interpretation no longer appears so convincing. In fact, ν_4 of PH$_3$ also has a two-dimensional symmetry representation, so it is also doubly degenerate, and then like for ν_4 of CHCl$_3$, if we divide by 2 the quenching efficiency of PH$_3$, we obtain again at $\Delta\nu = 20.4$ cm^{-1} of Figure 10 a point, represented by the ▽ (downward open triangle) symbol, lying on the straight line. ν_4 is thus the only mode responsible for V−V energy exchange with PH$_2$(ν_2'' = 1).

On the other hand, in a more accurate consideration, the coexistence of two vibrational modes capable, each one separately, of exchanging energy with PH$_2$($\nu_2'' = 1$) with different efficiencies does not mean that in a collision both of them are operative at the same time, producing a global efficiency that is the sum of their separate efficiencies. It is rather more probable that the vibrational mode with higher efficiency predominates, giving rise to the measured experimental effect.

With what has been discovered about the degenerate vibrations of the quencher in mind, the molecule CH$_4$ has been selected for investigation. CH$_4$ has two vibrational modes ν_4 and ν_2 capable of carrying out V−V exchange with PH$_2$($\nu_2'' = 1$), with $\Delta\nu = -204$ cm^{-1} for ν_4 and $\Delta\nu = -432$ cm^{-1} for ν_2. On the simple basis of these different $\Delta\nu$, Figure 10 shows that the efficiency of ν_2 should be ≈$^1/_3$ of that expected for ν_4, but according to what has just been said above for PH$_3$, ν_2 should not contribute to the overall deactivation of PH$_2$($\nu_2'' = 1$). ν_4 is particularly interesting because it belongs to f symmetry species, i.e., its symmetry representation is three-dimensional. ν_2 instead is an e symmetry species. ν_4 is thus a triply degenerate vibration, and from what has been illustrated above with CHCl$_3$, the quenching efficiency of this vibrational mode should be three times that expected from the line of Figure 10 in the case where ν_4 is a nondegenerate vibration. The experimental data, however, is quite surprising. The data lies right on the straight line of Figure 10 as any other molecule with a one-dimensional symmetry representation for the modes that participate in V−V exchange with PH$_2$($\nu_2'' = 1$).

The explanation of this fact should lie in the lifetime of the collision complex. If the complex lives long enough, as presumably is the case with CHCl$_3$, PH$_2$($\nu_2'' = 1$) could have the chance to exchange its excitation energy with both the $\nu_4 = 0$ levels of the doubly degenerate ν_4 mode of CHCl$_3$, and thus the quenching efficiency results enhanced by a factor 2. With CH$_4$, it is true that, in the encounter between this molecule and PH$_2$, this latter should come in touch with all three of the $\nu_4 = 0$ levels of the triply degenerate ν_4 mode of CH$_4$, but the lifetime of the complex should be so short that PH$_2$($\nu_2'' = 1$) could have the chance of releasing energy to only one of the

degenerate ν_4 vibrations, and then the complex redissociates again with the net result of ν_4 of CH_4 behaving as a non-degenerate mode. The short-lived complex of CH_4 and PH_2 is confirmed by the rare-gas-like behavior of CH_4 that we have seen above in the quenching of $PH_2(\tilde{A}^2A_1; \nu_2' = 0$ and 1).

Thus, in the case of degenerate vibrations, the other condition for an enhancement of the V−V efficiency to occur is a sufficiently long collision complex lifetime.

The linear relationship between log values of deactivation probability of $PH_2(\tilde{X}^2B_1; \nu_2'' = 1)$ and $\Delta\nu$ appears thus well established.

4. Conclusion

With the quenching molecules investigated in the present work, the available data are sufficient enough to give a reliable picture of the quenching of $PH_2(\tilde{A}^2A_1; \nu_2' = 0$ and 1) and to try an interpretation with the existing models.

It appears that none of these theories, Parmenter and co-workers' theory, Thayer and Yardley's theory, or complex formation theory, gives a satisfactory correlation for the whole mass of data.

All of these models correlate very well the rare gas quenchers and some nonpolar molecules. The correlation line according to Parmenter et al. has helped to quantify the deviations of the polar data and to attempt an explanation of these deviations.

The vibration relaxation data of $PH_2(\tilde{X}^2B_1; \nu_2'' = 1)$ by polyatomic molecules give a very interesting picture of the V−V process. We have been able to reliably establish a linear relationship between the log values of deactivation probability and the energy gap $\Delta\nu$ for nondegenerate quencher vibrational modes. This linear relationship has permitted revealing of a certain number of important phenomena: the enhancement of the efficiency of V−V energy exchange by inversion in NH_3 and by the degenerate vibrational modes of the quencher, which participate in the process. The latter effect, however, is not always operative as in the case of CH_4 quencher. This has been explained by the insufficiently long lifetime of the collision complex $[PH_2- CH_4]$.

References and Notes

(1) Nguyen Xuan, C. *Chem. Phys. Lett.* **2005,** *406***,** 415**.**
(2) Nguyen Xuan, C.; Margani, A. *J. Phys. Chem. A* **2002,** *106*, 5202, and references therein.
(3) Lin, H. M.; Seaver, M.; Tang K. Y.; Knight, A. E. W.; Parmenter, C. S. *J. Chem. Phys.* **1979,** *70,* 5442**.**
(4) Thayer, C. A.; Yardley, J. T. *J. Chem. Phys.* **1972,** *57*, 3992.
(5) Holtermann, D. L.; Lee, E. K. C.; Nanes, R. *J. Chem. Phys.* **1982,** *77*, 5327.
(6) Nguyen Xuan, C.; Margani, A.; Mastropietro, M. *J. Chem. Phys.* **1997,** *106*, 8473.
(7) Nguyen Xuan, C.; Margani, A. *Chem. Phys. Lett.* **2000,** *321*, 328.
(8) L'Air Liquide. *Encyclopédie des Gas*; Elsevier: Amsterdam, 1976.
(9) Nguyen Xuan, C.; Margani, A. *J. Chem. Phys.* **1990,** *93*, 136.
(10) Yardley, J. T. *Introduction to Molecular Energy Transfer*; Academic: New York, 1980.
(11) Hirschfelder, J. O.; Curtiss, C. F.; Byron Bird, R. *Molecular Theory of Gases and Liquids*, 4th printing; Wiley: New York, 1967.
(12) Nguyen Xuan, C.; Margani, A. *J. Chem. Phys.* **1998**, *109*, 9417.
(13) Fairchild, P. W.; Smith, G. P.; Crosley, D. R. *J. Chem. Phys.* **1983**, *79*, 1795.
(14) Stogryn, D. E.; Stogryn, A. P. *Mol. Phys.* **1966**, *11*, 371.
(15) Khristenko, S. V.; Maslov, A. I.; Shelveko, V. P. *Molecules and Their Spectroscopic Properties*; Springer: Berlin, 1998.
(16) Chan, S. C.; Rabinovitch, B. S.; Bryant, J. T.; Spicer, L. D.; Fujimoto, T.; Lin, Y. N.; Pavlou, S. P. *J. Phys. Chem.* **1970**, *74*, 3160.
(17) Ed., Weast, R. C. *Handbook of Chemistry and Physics*, 66th ed.; CRC Press Inc.: Boca Raton, FL, 1985−1986.
(18) Berkowitz, J.; Curtiss, L. A.; Gibson, S. T.; Greene, J. P.; Hillhouse, G. L.; Pople, J. A. *J. Chem. Phys.* **1986**, *84*, 375.
(19) Russell, A. J.; Spackman, M. A. *Mol. Phys.* **1997**, *90*, 251.
(20) Hofzumahaus, A.; Stuhl, F. *J. Chem. Phys.* **1985**, *82*, 3152.
(21) Koplitz, B.; Xu, Z.; Baugh, D.; Buelow, S.; Häuler, D.; Rice, J.; Reisler, H.; Qian, C. X. W.; Noble, M.; Wittig, C. *Faraday Discuss. Chem. Soc.* **1986**, *82*, 125.
(22) Callear, A. *Appl. Opt. Suppl.* **1965**, *2*, 145.
(23) Herzberg, G. *Molecular Spectra and Molecular Structure III. Electronic Spectra and Electronic Structure of Polyatomic Molecules*; Van Nostrand: Princeton, NJ, 1967.
(24) Shimanouchi, T. *Tables of Molecular Vibrational Frequencies, Consolidated Volume 1*; NSRDS-NBS 39; National Bureau of Standards: U.S. Department of Commerce, 1972.